ACS Chemical Neuroscience

Research Article

pubs.acs.org/chemneuro

Conformational Compatibility Is Essential for Heterologous Aggregation of α-Synuclein

Arshdeep Sidhu,[†] Ine Segers-Nolten,[†] and Vinod Subramaniam*[,†,‡,§]

[†]Nanobiophysics, MESA+ Institute for Nanotechnology, [‡]MIRA Institute for Biomedical Technology and Technical Medicine, University of Twente, 7522 NB Enschede, The Netherlands

[§]Vrije Universiteit Amsterdam, De Boelelaan 1105, 1081 HV Amsterdam, The Netherlands

Supporting Information

ABSTRACT: Under aggregation-prone conditions, soluble amyloidogenic protein monomers can self-assemble into fibrils or they can fibrillize on preformed fibrillar seeds (seeded aggregation). Seeded aggregations are known to propagate the morphology of the seeds in the event of cross-seeding. However, not all proteins are known to cross-seed aggregation. Cross-seeding has been proposed to be restricted either because of differences in the protein sequences or because of conformations between the seeds and the soluble monomers. Here, we examine cross-seeding efficiency between three α-synuclein sequences, wild-type, A30P, and A53T, each varying in only one or two amino acids but forming morphologically distinct fibrils. Results from bulk Thioflavin-T measurements, monomer incorporation quantification, single fibril fluorescence microscopy, and atomic force microscopy show that under the given solution conditions conformity between the conformation of seeds and monomers is essential for seed elongation. Moreover, elongation characteristics of the seeds are defined by the type of seed.

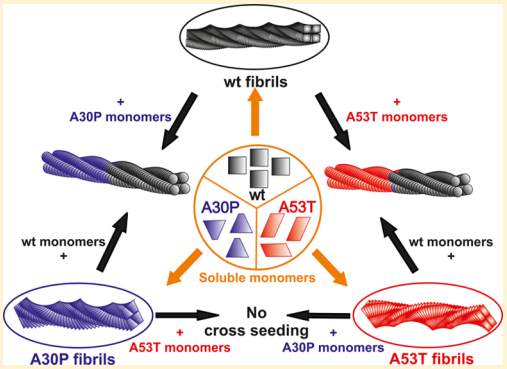

KEYWORDS: *Seed and monomer conformation, sequence similarity, heterologous seeding, templating, α-synuclein, two-color fluorescence microscopy*

Misfolded protein aggregates are associated with a number of degenerative diseases.[1] Initiation of protein aggregation *in vivo* is not well understood; however, it is believed that once initial aggregates are formed in a few cells they persist due to resistance to degradation or aberrations in protein degradation pathways.[2−4] The presence of misfolded proteins is suggested to induce misfolding in nascent polypeptides of the same (homologous) and different sequences (heterologous/cross-seeding).[5] Homologous and heterologous seedings are recognized as a key accelerators of *in vivo* aggregation of soluble monomers and are proposed to be the main mechanism for the spread of the associated pathology.[5−9] *In vitro* seeded experiments are oversimplified models of *in vivo* aggregation; however, they can be instrumental in identifying factors that promote or inhibit cross-seeding.

In seeded aggregations, the nucleation phase, represented by a lag phase, is bypassed, leading to spontaneous exponential fibrillization of the soluble monomers.[9−11] In α-synuclein (αSyn), a 140 amino acid neuronal protein associated with Parkinson's disease (PD), the elongation of the seeds is proposed to occur by the addition of monomers to the elongating end(s).[12,13] In amyloid-β (Aβ) and αSyn aggregations, the aggregating monomer is suggested to template on the seed and result in the propagation of structural information.[14,15] Unlike homologous fibrillization, in heterologous fibrillization not all amyloidogenic proteins are known to cross-seed aggregation. Sequence similarity and conformational compatibility are believed to be two principal factors that govern cross-seeding.[16] In the case of hen egg white lysozyme, sequence similarity has been suggested to be critical for cross-seeded aggregation with other proteins.[17] However, poor cross-seeding between Aβ and islet amyloid polypeptide (IAPP), which share high sequence similarity, highlights the importance of the molecular conformations of the seeds and the monomers.[16] Therefore, like most other amyloid features, cross-seeding characteristics vary among different amyloidogenic proteins.

In PD, in addition to wild-type (wt) αSyn, which is implicated in idiopathic PD, a number of point mutations are documented for the familial form. The point mutations known so far, A30P, E46K, H50Q, G51D, A53T, and A53E, are reported to be autosomal dominant point mutations, where the presence of a single copy of the mutant gene can lead to disease conditions.[18−23] In heterozygous individuals carrying a mutant allele, both wt and mutant αSyn are expressed. In such a situation, the presence of two different protein sequences can be imagined to modulate aggregation by cross-seeding. For αSyn, wt and A30P are shown to cross-seed aggregations, suggesting that high sequence identity can give rise to similar

Received: December 7, 2015
Accepted: March 19, 2016
Published: March 19, 2016

DOI: 10.1021/acschemneuro.5b00322
ACS Chem. Neurosci. 2016, 7, 719−727

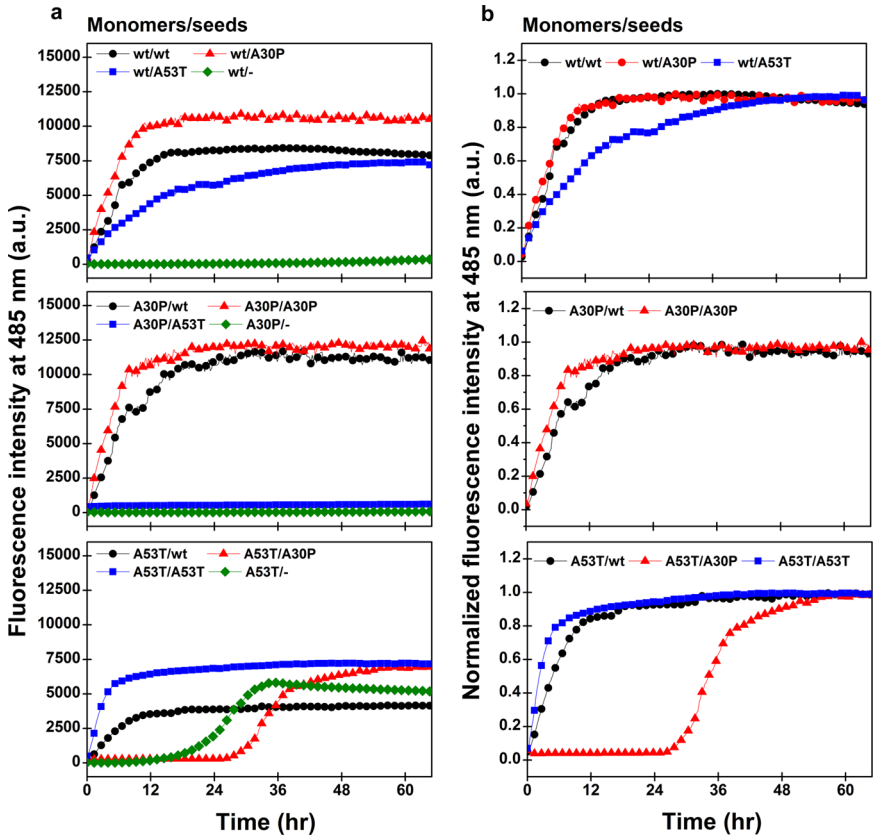

Figure 1. ThT fluorescence representing the kinetics of homologous and heterologous seeded aggregations. (a) Measured fluorescence intensities. Unseeded aggregations are included as reference. (b) Fluorescence intensities of the seeded aggregations, normalized to the maximum intensity measured at the plateau phase per curve. The A30P/A53T aggregation curve is not shown because the plateau phase was not reached. For clarity, only one representative curve from the triplicate is shown for each aggregation reaction.

conformations,[24] whereas mutual enhancement of αSyn and tau aggregation points toward conformation-dependent cross-seeding in unlike peptide sequences.[25,26] In addition, a recent study investigating the effect of different strains (polymorphs) of αSyn on tau aggregation proposes that seeding efficiency is strain-specific, underscoring the importance of subtle structural differences in templating fibrillization.[27] The distinct polymorphs in Aβ and αSyn fibrils have been reported to manifest characteristic molecular conformations.[14,15,28−30] Thus, differences between the protein conformation in the fibrils/seeds and the conformations amenable to the soluble monomer may be critical for determining the efficacy of cross-seeding between proteins with or without high sequence similarity.

To probe this hypothesis, we systematically performed heterologous and homologous seeded aggregations among three αSyn sequences (wt, A30P, and A53T) that have very high sequence similarity but form fibrils of different morphologies under the same solution conditions. The solution conditions that we use were based on our previous study that yielded homogeneous[31] but distinct polymorphs of wt, A30P, and A53T fibrils at the plateau phase of the Thioflavin-T (ThT) assay. Analyses of the heterologous and homologous seeded aggregations based on the ThT fluorescence assay, residual monomer concentration (RMC), and atomic force microscopy (AFM) showed that seeding is most efficient between the seeds and monomers of the same sequence. Moreover, A30P and A53T seeds with contrasting morphology do not cross-seed aggregation of A53T and A30P monomers, respectively. Studies examining the elongation of seeds at the single-fibril level with two-color fluorescence microscopy revealed that the elongation characteristics of the seeds are type-specific, in addition to corroborating the bulk experiments.

RESULTS AND DISCUSSION

Elongation of αSyn seeds is proposed to occur primarily through addition of monomers on the end(s).[12] The extent and the rate of elongation in a seeded aggregation reflect the efficiency with which the soluble monomer can be incorporated at the end of the seeds. Therefore, differences in the fold or conformation of the seed and the conformations accessible to monomers are likely to affect the elongation of the seed. A30P and A53T αSyn monomers self-assemble into fibrils of distinct morphologies under uniform solution conditions (10 mM Tris-HCl, 10 mM NaCl, and 0.1 mM EDTA, pH 7.4; Supporting Information Figure S1). ssNMR studies suggest that physicochemical and conformational differences underlie the morphological differences observed in αSyn fibrils.[15,30,32] Thus, discrete morphologies of A30P and A53T αSyn fibrils likely present a sequence-based conformational difference. Assuming that under the given solution conditions the monomers of A30P and A53T αSyn prefer select conformations, which result in nearly homogeneous fibrils with a characteristic morphology, monomers of A30P and A53T may not fibrillize equally well on seeds of different conformations, i.e., A53T and A30P. To probe this hypothesis, we performed homologous and heterologous seeded aggregations with wt, A30P, and A53T αSyn.

DOI: 10.1021/acschemneuro.5b00322
ACS Chem. Neurosci. 2016, 7, 719−727

Fibrillization of wt αSyn and Its Disease Mutants. Wild-type αSyn and its disease mutants (A30P and A53T) were fibrillized *de novo,* in 10 mM Tris-HCl, 10 mM NaCl, and 0.1 mM EDTA, at pH 7.4, to be used as seeds. The morphologies of the produced fibrils were determined by AFM. Wild-type fibrils showed a periodic twist (p) of about 100 nm. A30P exhibited $p \sim 100$ nm, whereas A53T fibrils showed $p \sim 350$ nm and/or heterogeneous fibrils (Supporting Information Figure S1).

Aggregation Kinetics of αSyn in Homologous and Heterologous Fibrillization. Homologous aggregations were set up with wt/A30P/A53T seeds and wt/A30P/A53T monomers. Heterologous aggregations were set up using wt monomers with A30P or A53T seeds, A30P monomers with wt or A53T seeds, and A53T monomers with wt or A30P seeds.

In homologous aggregations, all of the reactions lacked the lag phase, which is characteristic of a seeded aggregation. The kinetics of the aggregations was quantified from triplicates by reading the time required to reach half of the maximum fluorescence intensity (half-time, $t_{1/2}$). A53T homologous aggregations showed the shortest $t_{1/2}$ of 2.3 ± 0.2 h, followed by A30P with 4.0 ± 0.2 h and wt with 5.4 ± 0.4 h (Figure 1 and Table 1).

Table 1. Summary of the Determined Half-Time for Homologous and Heterologous Seeded Aggregations[a]

$t_{1/2}$ (h)		monomers		
		wt	A30P	A53T
seeds	wt	5.4 ± 0.4	5.7 ± 0.2	6.2 ± 1.2
	A30P	4.3 ± 0.2	4.0 ± 0.2	35.0 ± 1.5
	A53T	9.7 ± 1.0		2.3 ± 0.2

[a]Data are shown in hours (±SD among triplicates).

In heterologous aggregations, wt monomers fibrillized faster on A30P seeds in comparison to that on A53T seeds ($t_{1/2}$ = 4.3 ± 0.2 and 9.7 ± 1.0 h, respectively). A30P monomers aggregated on wt seeds with a $t_{1/2}$ of 5.7 ± 0.2 h, whereas they did not appear to grow at all on A53T seeds (based on the ThT assay up to the experimental time of 65 h). A53T monomers fibrillized in the presence of wt seeds with a $t_{1/2}$ of 6.2 ± 1.2 h. Aggregation of A53T monomers with A30P seeds showed a clear lag phase, which is aberrant for a seeded aggregation (Figure 1a). The lag phase was determined to be 26.2 ± 3.1 h by the intercept of the extrapolated baseline and the slope of the exponential phase. The $t_{1/2}$ determined for the A53T monomer/A30P seed aggregation was 35.0 ± 1.5 h (Table 1). Thus, based on the ThT fluorescence intensity, in heterologous reactions, wt monomers fibrillized with both A30P and A53T seeds, whereas the two mutant monomers aggregated only on wt seeds. However, it is notable that between homologous and heterologous aggregations all three αSyn seeds grew fastest with homologous monomers. These results indicate that seeds elongate more efficiently with monomers that have the same sequence and secondary/tertiary structure.

ThT assays alone are not reliable indicators of the extent of amyloid formation in fibrillization reactions.[33] Thus, to ascertain that the relative fibrillization curves obtained with ThT fluorescence assays correlate with the conversion of monomers into fibrils, we determined the RMC for all of the aggregation reactions.

Residual Monomer Concentration. On the basis of the amount of soluble monomers present at the end of an aggregation reaction, the extent of monomers incorporated into the fibrils can be determined. We calculated the RMC at 65 h by measuring the absorbance at 280 nm (A_{280nm}), including a correction for the contribution of soluble oligomers based on the scatter signal detected at 330 nm as A_{330nm}.[34]

In homologous aggregations, wt and A53T samples showed a conversion of about 92% of the monomers into fibrils (Table 2). A30P samples revealed a lower conversion of about 79%,

Table 2. RMC for Homologous and Heterologous Aggregation Reactions[a]

RMC (μM)		monomers		
		wt	A30P	A53T
seeds	wt	8 ± 2	23 ± 2	3 ± 3
	A30P	20 ± 3	21 ± 4	6 ± 1
	A53T	25 ± 1	82 ± 2	8 ± 2

[a]Data are in micromolar (±SD among triplicates).

although the final fluorescence intensity of the A30P sample is considerably higher than that of wt or A53T fibrils (Figure 1a), again highlighting that the total fluorescence intensity in ThT assays can be misleading.

In heterologous aggregations, consistent with the ThT results, the wt monomers fibrillized on A30P seeds and A53T seeds well, with about 80 and 75% monomer conversion, respectively. Around 77% of the A30P monomers added to the wt seeds, whereas most of the A30P monomers (~82%) with A53T seeds remained soluble. The inability of A53T seeds to seed aggregation of A30P monomers, as observed in ThT assays and RMC determinations, is suggestive of an incompatibility between the seed conformation and the conformations favored by the soluble monomers. A53T monomers showed a high incorporation into fibrils with wt seeds (~97%) and A30P seeds (~94%). Conversion of most of the A53T monomers (94%) into fibrils by growing on A30P seeds is, however, unlikely because the ThT curve shows a distinct lag phase. The lag phase for A53T monomers and A30P seeded aggregation is longer than the lag phase observed for unseeded (negative control) A53T aggregation (~18 h). Therefore, it is possible that the fibrillization observed in this seeded aggregation is due to *de novo* aggregation of A53T monomers and not because of fibrillization of A53T monomers on A30P seeds. To test this assumption, we determined if the fibrils in the seeded aggregation had a morphology typical of A53T fibrils.

Atomic Force Microscopy Imaging. AFM images showed that the A30P and A53T fibrils used as seeds in these experiments had distinct morphologies. A30P fibrils show periodicities of ~100 nm, whereas A53T fibrils exhibit periodicities of ~350 nm along with heterogeneous fibrils (Supporting Information Figure S1). Seeded aggregations in Aβ and αSyn have been proposed to reproduce the morphology of the seeds.[14,32] Therefore, if the fibrils formed in the A53T monomer/A30P seeded aggregation are formed due to templating by the seed, then they should display the morphology characteristic of A30P fibrils (i.e., with $p \sim 100$ nm). However, if the fibrils arise due to *de novo* fibrillization of A53T monomers, then they should exhibit the morphology typical for A53T fibrils under the given aggregation conditions ($p \sim 350$ nm and/or heterogeneous fibrils). Fibrils from the

DOI: 10.1021/acschemneuro.5b00322
ACS Chem. Neurosci. 2016, 7, 719−727

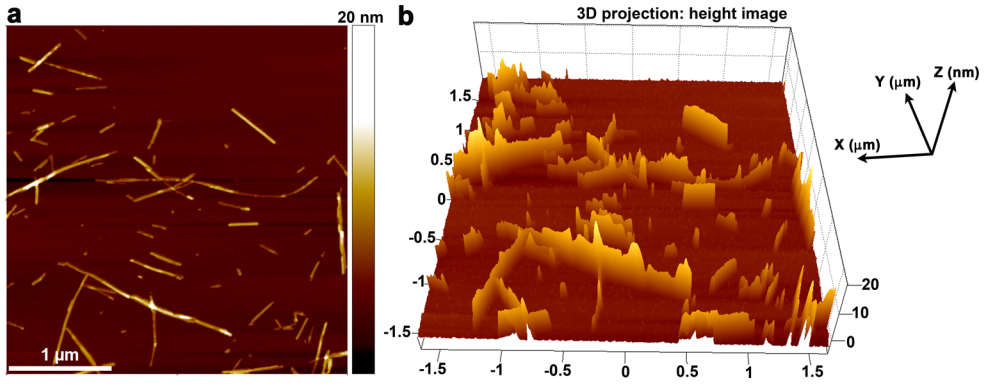

Figure 2. AFM height image of A53T monomers aggregated in the presence of A30P seeds. The fibrils show morphology typical for A53T fibrils. (a) Height image; (b) 3D projection of the height image. 3D images were prepared by standard settings in SPIP.

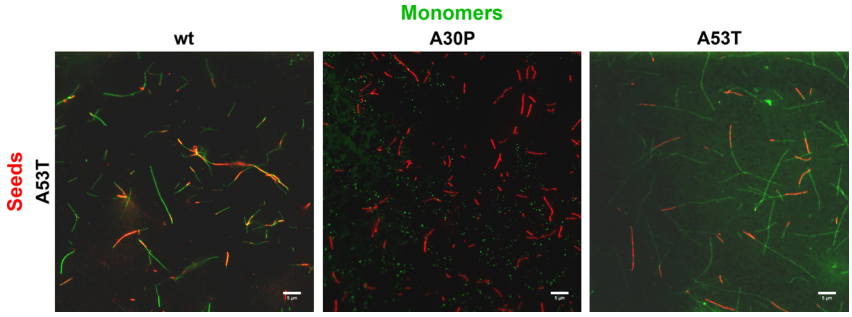

Figure 3. Representative overview images of A53T seeded aggregations with wt, A30P, and A53T monomers, showing seeds labeled with AF 647 and extensions visualized by *ex situ* bound ThT. Scale bar: 5 μm.

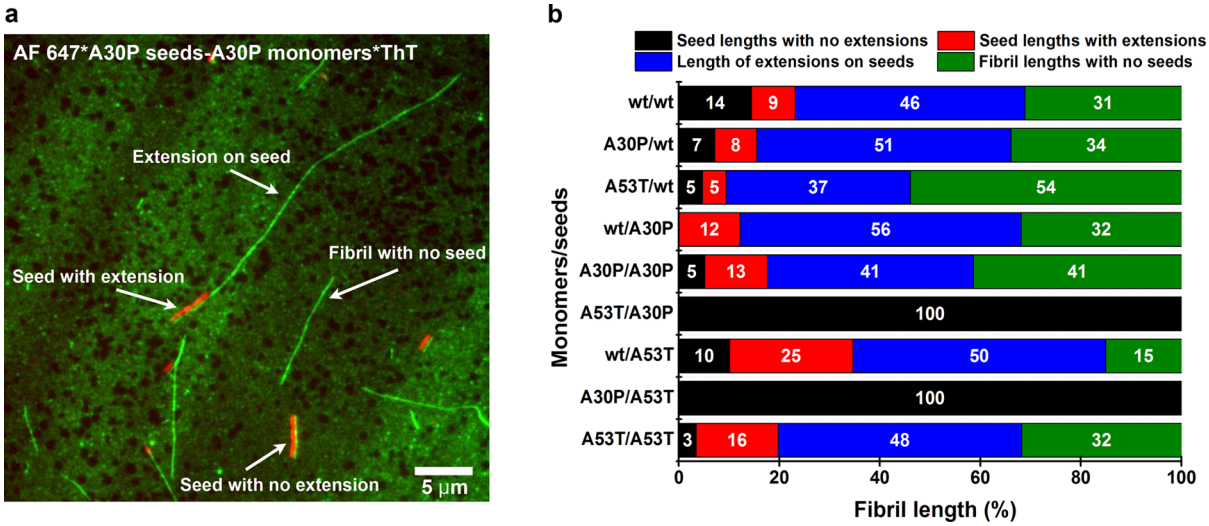

Figure 4. (a) Representative wide-field fluorescence image exemplifying the various types of fibril lengths analyzed. Seeds were labeled with AF 647, and the extensions were visualized by *ex situ* binding of ThT. Small red−green color shifts result from a slightly different optical path when using different filter cubes. Scale bar: 5 μm (b) Histogram showing the percentage fibril lengths from different seeded aggregation reactions. Around 1 mm of total length was measured for all aggregations. For seeds with bidirectional growth, both of the extensions were included in the analyses as "length of extensions with seeds".

A53T monomer/A30P seeded aggregations exhibit the morphology of A53T fibrils and not of A30P fibrils (Figure 2 and Supporting Information Figure S1). Therefore, the fibrils are formed by *de novo* fibrillization of monomeric A53T and not by templated growth on the A30P seeds. This result explains the lag phase observed in the ThT fluorescence assay. It also shows that A30P and A53T αSyn do not cross-seed each other. The marked selectivity in fibrils to act as seeds again points toward incompatibility between the conformations at the seed ends and the conformations favored by the soluble monomers. To gain a better understanding of seed elongation with respect to the compatibility of the seed and monomer, we imaged fibrils by fluorescence microscopy to assess fibril growth at the single-fibril level.

Choice of Fluorophore. Visualization of amyloid fibrils by fluorescence microscopy routinely employs fibrils covalently

DOI: 10.1021/acschemneuro.5b00322
ACS Chem. Neurosci. 2016, 7, 719−727

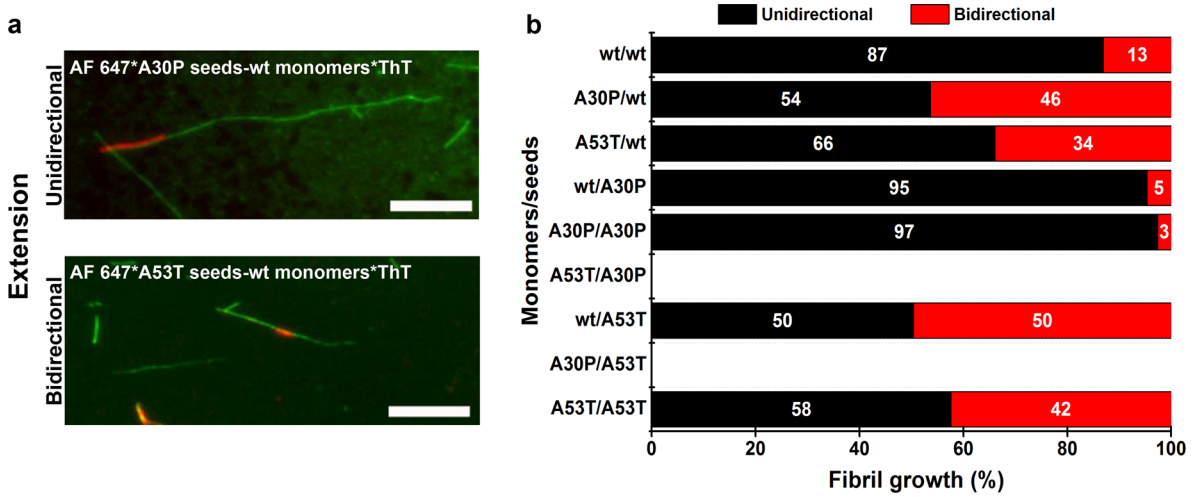

Figure 5. (a) Representative wide-field fluorescence images showing uni- and bidirectional elongation of seeds. Seeds were labeled with AF 647, and the extensions were visualized by *ex situ* binding of ThT. Scale bar: 5 μm. (b) Histogram showing the proportions of uni- and bidirectional growth in different seeded aggregations.

labeled with fluorophores. Alexa Fluor (AF) fluorophores are some of the most commonly used fluorescent probes and are available with a variety of linkers. Previously, amyloid fibrils labeled with different AF dyes have been used to study the growth symmetry at both ends during elongation.[35,36] These studies also show that the fluorescent labeling of the seeds did not affect the aggregation kinetics of αSyn and insulin. For our fluorescence experiments, which aim at probing a possible preference for specific monomer conformations for seed elongation, it is important to exclude a fluorophore-dependent effect as much as possible. Therefore, we first prepared AF 488 and AF 647 labeled wt-A140C fibrils and compared their length distributions. The labeled fibrils were prepared in a seeded aggregation (2 μM wt seeds) from a mixture of 10 μM AF labeled wt-A140C monomers and 88 μM unlabeled wt monomers. The mean length of the fibrils labeled with AF 488 (1.2 $\pm$ 1.0 μm) was about 1 μm shorter than that of the AF 647 labeled fibrils (2.1 $\pm$ 1.2 μm) (Supporting Information Figure S2). Although the mean fibril lengths are not decidedly different with the AF dyes used, the results indicate that a dye effect cannot be ruled out. Therefore, to avoid potential fluorophore-biased fibril elongation, we used AF 647 labeled seeds in combination with unlabeled monomers and imaged the grown extensions by fluorescence of *ex situ* bound ThT.

Fibril Length Analyses. Wild-type, A30P, and A53T monomers carrying a cysteine residue at their C-terminus (substituting alanine at position 140) were labeled with AF 647 dye, and 10 μM labeled monomers were aggregated with 90 μM unlabeled monomers of the same sequence in 10 mM Tris-HCl, 10 mM NaCl, and 0.1 mM EDTA at pH 7.4 to produce fibrils to be used as seeds. Next, homologous and heterologous aggregations were set up under quiescent conditions to avoid fibril fragmentation. After 24 h, samples were prepared for wide-field fluorescence microscopy (Figure 3). The images were analyzed for fibrillization of the monomers by uni- or bidirectional growth of the seed, for seeds with no elongation, and for fibrils without seeds. In all samples, about 1 mm of total fibril length was analyzed.

Homologous Aggregations. In homologous aggregations, 40−50% of the total (new) fibril length was linked to the seeds, whereas about 30% of the fibril length did not show the presence of any seed (Figure 4). The fibrils that are not associated with seeds are most likely fragments of the extensions grown on seeds because none of the αSyn sequences studied shows *de novo* fibrillization in 24 h under quiescent aggregation conditions. A higher percentage of seeds appears to participate in fibrillization in A30P and A53T aggregations, in comparison to that with wt seeds, as only 5 and 3% of the total fibril lengths correspond to seeds with no extensions. Wild-type aggregation showed a higher percentage, 14%, of unextended seeds, apparently correlating with the relatively slower aggregation observed in the ThT assay (Figures 1 and 4). However, since the precise fibril concentration in the samples is unknown, it is difficult to draw accurate conclusions on the fraction of seeds that elongates. The average length of the seed extension for wt fibrils was 9.0 $\pm$ 3.4 μm. The average length for A30P and A53T aggregations were similar, 9.9 $\pm$ 7.1 and 7.5 $\pm$ 5.1 μm, respectively. The length distribution for A30P and A53T extension was, however, broader in comparison to that of wt (Supporting Information Table S1).

Heterologous Aggregations. In heterologous aggregations, wt monomers appeared to grow well on both A30P and A53T seeds, with close to 50% of the total fibril lengths linked with growth on the seeds. However, the average length of a wt fibril grown on an A30P seed is almost 5 times (15.6 $\pm$ 9.9 μm) the average length of a wt fibril grown on an A53T seed (3.9 $\pm$ 2.2 μm). The A30P monomers fibrillized on wt seeds account for ~50% of the total fibril lengths. In aggregations with A53T monomers and wt seeds, ~37% of the fibril lengths were associated with seeds and around 54% did not show any seed. In agreement with the ThT assay, RMC, and AFM imaging, A30P and A53T seeds did not show any elongation in the presence of A53T and A30P monomers, respectively (Figures 3 and 4 and Supporting Information Table S1). These results establish that the conformations of A30P and A53T seeds are not conducive for sustained addition and elongation of A53T and A30P monomers, respectively. The A30P and A53T variants and wt αSyn differ by one amino acid in their sequences, whereas the two disease-related variants differ by two amino acids with respect to each other. Although sequence may play a role in cross-seeding, the sum of our data leads us to postulate that the minor difference in the sequence translates

DOI: 10.1021/acschemneuro.5b00322
ACS Chem. Neurosci. 2016, 7, 719−727

into conformational/structural differences that form the basis of our observations.[24,37,38] In light of the dock and lock mechanism for the elongation of fibrils,[39−41] it is probable that the monomers tether at the ends of the seeds (lock) but are unable to fold into growth-favoring conformations. Thus, elongation is blocked altogether.

Kinetics of Seed Extension. An evident feature of seed elongation, irrespective of the monomer, is the broad distribution of the fibril lengths per seed (Supporting Information Figure S3). The broad distribution suggests heterogeneous rates of seed elongation. Heterogeneity in the elongation rates has been proposed to be a consequence of the "stop and go" growth mechanism.[35,41−44] The stop and go mechanism outlines the possible eventualities of the docking step in the lock and dock mechanism of growth. Once a monomer is docked at the fibril end, it may acquire the template fold and contribute to the fibril growth ("go") or it may fail to do so and stall the growth intermittently or permanently ("stop"). In the case of intermittent stalling of elongation, the growth rate of each end of the seed could be different, leading to heterogeneous growth rates, as observed in the present study. Furthermore, in the case of large differences in the conformation of the seed and the soluble monomer, it is likely that soluble monomers do not bind to the seeds at all, as seen in the aggregation between A30P/A53T seeds and A53T/A30P monomers, respectively.

Directionality of Seed Extension. An additional aspect of seed elongation is the elongation rate at the two sides of the seeds. The elongation rate of a seed is believed to depend on the ratio of molecular association and dissociation at the fibril ends.[45] Since the two ends are formed of the same protein unit, one could reasonably expect each end to be equivalent. However, several studies on amyloids propose asymmetric seed elongation.[35,36,44,46,47] In our study, a comparison between the different types of seeds show that the aggregations with wt and A30P seeds primarily elongate in a unidirectional manner. The fibrillizations with A53T seeds, in contrast, showed about 50% unidirectional and 50% bidirectional fibril growth (Figure 5). However, the length of the two extensions on all of the seeds exhibiting bidirectional growth was not similar, i.e., one side was always longer than the other. The molecular interfaces at both ends of the fibril are, however, identical, which implies that the same free energy is associated with monomer addition at both ends. Despite there being an analogous ratio of the monomer's on and off rates at both ends, topological or stereochemical constraints most likely cause the fibril elongation rates to differ.[44,48,49] In all, the growth patterns observed among the different seeds indicate that the type of seed governs the symmetry of seed elongation.

Overall, the results show that in αSyn seeded aggregation reactions, under the given solution conditions, conformational compatibility between the seed and the soluble monomer is important for seed elongation. Although αSyn is characterized as an intrinsically disordered protein, the monomers likely exist in dynamic ensembles in a collapsed coil state (with long-range intramolecular interactions).[50,51] The distribution of the ensembles is critically influenced by the solution conditions. In addition, a single amino acid difference in the protein sequence can lead to pronounced variation in the thermodynamically favorable conformations.[52,53] Therefore, under particular solution conditions, minor variations in the polypeptide sequence can result in fibrils of distinct morphology. While heterologous aggregations between seeds and monomers of conflicting conformation deter elongation of seeds, in the event of cross-seeding the aggregation characteristics are determined by the properties of the seeds. The observed conformational stringency for seed elongation may have implications for *in vivo* propagation of amyloids and strain selection, as conformation and not sequence appears to be key for inducing aggregation in soluble αSyn.

METHODS

αSyn Expression and Purification. Wild-type, A30P, A53T, and cysteine carrying mutants of wt (wt-A140C), A30P (A30P-A140C), and A53T (A53T-A140C) were used in the present study. The cysteine carrying mutants were generated using QuikChange II site-directed mutagenesis kits (Agilent Technologies). All sequences were expressed and purified using protocols described previously.[31]

Unlabeled αSyn Fibrillization for Monitoring Kinetics from ThT Fluorescence. *De Novo Aggregations.* Stocks (250 μM) of monomeric wt, A30P, and A53T frozen at −80 °C were thawed and fibrillized in *de novo* aggregation reactions with 100 μM unlabeled αSyn, 10 mM Tris-HCl, 10 mM NaCl, 0.1 mM EDTA, and 20 μM ThT, at pH 7.4. All reactions were prepared in triplicate with volumes of 400 μL each in 2 mL Lo-Bind round-bottom Eppendorf centrifuge tubes and were incubated at 37 °C with 500 rpm orbital shaking in an Eppendorf Thermomixer comfort. The fibrils produced were checked for their morphology by AFM and were used as seeds in subsequent seeded experiments. The seeds for aggregation were prepared by sonication of the fibrils in thin-walled PCR tubes for 2 min in a bath sonicator (Branson 1510).

Seeded Aggregations: Homologous and Heterologous. Fibrillization reactions were set up using 2 μM preformed fibrils as seeds and 98 μM unlabeled αSyn, 10 mM Tris-HCl, 10 mM NaCl, 0.1 mM EDTA, and 20 μM ThT, at pH 7.4. All reactions were prepared in triplicate in a 200 μL volume and incubated in 96-well plates with optically transparent bottoms (Nunc, Thermo Fisher Scientific), sealed with adhesive film (Viewseal, Greiner Bio One). The plates were incubated at 37 °C with orbital shaking in a Safire^2 microplate reader (Tecan). The aggregations were monitored using ThT fluorescence by 446 nm excitation, and the ThT fluorescence emission intensity (bottom reading) was followed at 485 nm. Readings were taken every 15 min.

Homologous aggregations were set up with wt/A30P/A53T seeds and wt/A30P/A53T monomers, respectively. Heterologous aggregations were set up using wt monomers with A30P or A53T seeds, A30P monomers with wt or A53T seeds, and A53T monomers with wt or A30P seeds.

Residual Monomer Concentration Determination. RMC was determined by centrifugation of 100 μL of the aggregated protein solution (65 h) at 21 000*g* at room temperature for 1 h in an IEC Micromax microcentrifuge (Thermo Fisher Scientific). The supernatant (50 μL) was removed, and the absorbance at 280 and 330 nm was measured on a NanoDrop ND-1000 spectrophotometer (Isogen Life Science). The absorption at 280 nm was corrected for scattering contributions (A_{330}) that possibly result from oligomeric assemblies before the RMC was calculated.[34]

Atomic Force Microscopy. AFM samples were prepared by adsorbing 20 μL of fibril sample, 5−10 times diluted in 10 mM Tris-HCl, 10 mM NaCl at pH 7.4, on freshly cleaved mica (Muscovite mica, V-1quality, EMS) for 4 min, followed by washing twice with 100 μL of fresh Milli-Q water and drying in a gentle stream of nitrogen gas. AFM images were acquired on a Bioscope Catalyst (Bruker) in soft tapping mode in air using a silicon probe, NSC36 tip B, with a force constant of 1.75 N/m (NanoAndMore). All images were captured with a resolution of 512 × 512 pixels per image with a scan rate of 0.5 Hz. Images were analyzed by Scanning Probe Image Processor (SPIP) 6.0.13 software (Image Metrology).

Alexa Fluor Labeling of Monomers. Maleimide-functionalized AF dyes, AF 488 and AF 647, were dissolved in dry DMSO to prepare 25 mM stocks and stored at −80 °C in single-use aliquots. For assessing the effect of different AF dyes on fibril elongation, wt monomers

DOI: 10.1021/acschemneuro.5b00322
ACS Chem. Neurosci. 2016, 7, 719−727

carrying a cysteine at position 140 (alanine exchanged for cysteine) were labeled with AF 488 or AF 647.

Stocks (250 μM) of monomers were thawed and reduced with freshly prepared 1 mM DTT solution for 30 min at room temperature. Next, DTT was removed from the protein solution using a 2 mL Zeba spin desalting column (Pierce Biotechnology) following the manufacturer's protocol. Reduced and DTT-free monomers were immediately mixed with a 3 M excess of AF dye (thawed just before use). The reaction was mixed well and incubated for 1 h at room temperature in the dark. Next, excess unreacted dye was removed by two sequential steps of desalting by 2 mL Zeba spin columns. Stoichiometry/degree of labeling was determined by following the manufacturer's instructions, using extinction coefficients of 5745 (wt-A140C), 71 000 (AF 488), and 239 000 (AF 647) L mol^{-1} cm^{-1}. The calculated stoichiometry was 1.1 mol of dye per mole of protein (AF 488) and 2.3 mol of dye per mole of protein (AF 647).

For the seeded aggregation experiments, monomers of cysteine carrying mutants of wt (wt-A140C), A30P (A30P-A140C), and A53T (A53T-A140C) were labeled with AF 647 dye following the protocol described above. The stoichiometry of labeling was calculated to be 1.0, 2.2, and 1.7 mol of dye per mole of protein for wt-A140C, A30P-A140C, and A53T-A140C, respectively. The yield of labeled monomers in all reactions was about 80%.

Preparation of Alexa Fluor Labeled Fibrils. AF 488 and AF 647 Labeled wt-A140C Fibrils for Length Analysis. AF labeled fibrils were prepared by seeded aggregation (2 μM wt seeds) of 88 μM unlabeled wt αSyn monomers, 10 μM AF 488 or AF 647 labeled wt-A140C monomers, 10 mM Tris-HCl, 10 mM NaCl, and 0.1 mM EDTA, at pH 7.4. All reactions were prepared in triplicate with volumes of 400 μL each in 2 mL Lo-Bind round-bottom Eppendorf centrifuge tubes and were incubated at 37 °C with 500 rpm orbital shaking for 24 h in an Eppendorf Thermomixer comfort.

AF 647 Labeled Fibrils for Use as Seeds. AF labeled fibrils were prepared by fibrillization of 88 μM unlabeled wt/A30P/A53T αSyn monomers, 10 μM AF 647 labeled wt-A140C/A30P-A140C/A53T-A140C monomers, 10 mM Tris-HCl, 10 mM NaCl, and 0.1 mM EDTA at pH 7.4 in the presence of 2 μM wt/A30P/A53T seeds, respectively. All reactions were prepared in triplicate with volumes of 400 μL each in 2 mL Lo-Bind round-bottom Eppendorf centrifuge tubes and were incubated at 37 °C with 500 rpm orbital shaking for 72 h in an Eppendorf Thermomixer comfort.

Seeded Aggregations. Seeded aggregations were performed by combining 10 μM (based on initial monomer concentration) AF 647 labeled seeds and 90 μM unlabeled monomers. Aggregations were set up in 10 mM Tris-HCl, 10 mM NaCl, and 0.1 mM EDTA, at pH 7.4. All reactions were prepared in 400 μL volume in 2 mL Lo-Bind round-bottom Eppendorf centrifuge tubes and were incubated at 37 °C under quiescent conditions for 24 h.

Homologous aggregations were set up with wt/A30P/A53T seeds and wt/A30P/A53T monomers, respectively. Heterologous aggregations were set up using wt monomers with A30P or A53T seeds, A30P monomers with wt or A53T seeds, and A53T monomers with wt or A30P seeds.

Fluorescence Microscopy. Fibrils produced in the seeded aggregations were imaged by fluorescence microscopy. The seeds were visualized through AF 647 fluorescence, and the extensions were imaged through ThT fluorescence. Samples for fluorescence microscopy were prepared by placing 5 μL of 50−100 times diluted fibril samples containing 10 μM ThT on a clean microscope slide and covering the sample with a clean coverslip. The edges of the coverslip were sealed with lacquer, and the samples were allowed to settle for 24 h. Fluorescence images were acquired in wide-field mode using a Plan-Apo oil immersion objective with 100× magnification (NA = 1.45) from Olympus on a Nikon Eclipse Ti microscope equipped with a mercury arc lamp (Nikon Intensilight, C-HGFIE) for excitation. For imaging of AF 647 a filter cube consisting of a 590/650 nm band-pass excitation filter, a 660 nm long pass dichroic beam splitter, and a 662/737 nm band-pass emission filter was used. For imaging of ThT, a filter cube composed of a 445/465 nm band-pass excitation filter, a 458 nm long pass dichroic beam splitter, and a 470/500 nm band-pass emission filter was used. Fibril length analysis on fluorescence images was done using Simple Neurite tracer-Fiji software.[54]

■ ASSOCIATED CONTENT

Supporting Information

The Supporting Information is available free of charge on the ACS Publications website at DOI: 10.1021/acschemneuro.5b00322.

AFM height images and 3D projections, widefield fluorescence microscopy images, elongation histograms, and average fibril lengths (PDF)

■ AUTHOR INFORMATION

Corresponding Author

*E-mail: v.subramaniam@vu.nl.

Author Contributions

A.S., I.S.-N., and V.S. designed experiments. A.S. performed the experiments.

Funding

This work is supported by NanoNextNL, a micro- and nanotechnology consortium of the Government of The Netherlands and 130 partners. We also acknowledge support from the Foundation for Fundamental Research on Matter (FOM), which is part of Netherlands Organization for Scientific Research (NWO).

Notes

The authors declare no competing financial interest.

■ ACKNOWLEDGMENTS

The authors thank Kirsten van Leijenhorst-Groener, Yvonne Kraan, and Nathalie Schilderink for protein expression and purification and Prof. Mireille Claessens for valuable suggestions.

■ ABBREVIATIONS

αSyn, α-synuclein; AFM, atomic force microscopy; A30P-A140C, A30P αSyn protein sequence with residue 140 (alanine) substituted for cysteine; A53T-A140C, A53T αSyn protein sequence with residue 140 (alanine) substituted for cysteine; AF 488, Alexa Fluor 488; AF 647, Alexa Fluor 647; DMSO, dimethyl sulfoxide; PD, Parkinson's disease; RMC, residual monomer concentration; Wt-A140C, αSyn protein sequence with residue 140 (alanine) substituted for cysteine

■ REFERENCES

(1) Chiti, F., and Dobson, C. M. (2006) Protein misfolding, functional amyloid, and human disease. *Annu. Rev. Biochem. 75*, 333−366.

(2) Jucker, M., and Walker, L. C. (2013) Self-propagation of pathogenic protein aggregates in neurodegenerative diseases. *Nature 501*, 45−51.

(3) Knowles, T. P., Vendruscolo, M., and Dobson, C. M. (2014) The amyloid state and its association with protein misfolding diseases. *Nat. Rev. Mol. Cell Biol. 15*, 384−396.

(4) Perrett, R. M., Alexopoulou, Z., and Tofaris, G. K. (2015) The endosomal pathway in Parkinson's disease. *Mol. Cell. Neurosci. 66*, 21−28.

(5) Morales, R., Moreno-Gonzalez, I., and Soto, C. (2013) Cross-seeding of misfolded proteins: implications for etiology and pathogenesis of protein misfolding diseases. *PLoS Pathog. 9*, e1003537.

(6) Hilker, R., Brotchie, J. M., and Chapman, J. (2011) Pros and cons of a prion-like pathogenesis in Parkinson's disease. *BMC Neurol. 11*, 74.

DOI: 10.1021/acschemneuro.5b00322
ACS Chem. Neurosci. 2016, 7, 719−727

(7) Goedert, M., Spillantini, M. G., Del Tredici, K., and Braak, H. (2012) 100 years of Lewy pathology. *Nat. Rev. Neurol. 9*, 13−24.
(8) Goedert, M., Falcon, B., Clavaguera, F., and Tolnay, M. (2014) Prion-like mechanisms in the pathogenesis of tauopathies and synucleinopathies. *Curr. Neurol. Neurosci. Rep. 14*, 495.
(9) Harper, J. D., and Lansbury, P. T., Jr. (1997) Models of amyloid seeding in Alzheimer's disease and scrapie: mechanistic truths and physiological consequences of the time-dependent solubility of amyloid proteins. *Annu. Rev. Biochem. 66*, 385−407.
(10) Jarrett, J. T., and Lansbury, P. T., Jr. (1993) Seeding "one-dimensional crystallization" of amyloid: a pathogenic mechanism in Alzheimer's disease and scrapie? *Cell 73*, 1055−1058.
(11) Wood, S. J., Wypych, J., Steavenson, S., Louis, J. C., Citron, M., and Biere, A. L. (1999) alpha-synuclein fibrillogenesis is nucleation-dependent. Implications for the pathogenesis of Parkinson's disease. *J. Biol. Chem. 274*, 19509−19512.
(12) Buell, A. K., Galvagnion, C., Gaspar, R., Sparr, E., Vendruscolo, M., Knowles, T. P., Linse, S., and Dobson, C. M. (2014) Solution conditions determine the relative importance of nucleation and growth processes in alpha-synuclein aggregation. *Proc. Natl. Acad. Sci. U. S. A. 111*, 7671−7676.
(13) Spillantini, M. G., Crowther, R. A., Jakes, R., Hasegawa, M., and Goedert, M. (1998) alpha-Synuclein in filamentous inclusions of Lewy bodies from Parkinson's disease and dementia with lewy bodies. *Proc. Natl. Acad. Sci. U. S. A. 95*, 6469−6473.
(14) Petkova, A. T., Leapman, R. D., Guo, Z., Yau, W. M., Mattson, M. P., and Tycko, R. (2005) Self-propagating, molecular-level polymorphism in Alzheimer's beta-amyloid fibrils. *Science 307*, 262−265.
(15) Gath, J., Bousset, L., Habenstein, B., Melki, R., Bockmann, A., and Meier, B. H. (2014) Unlike Twins: An NMR Comparison of Two alpha-Synuclein Polymorphs Featuring Different Toxicity. *PLoS One 9*, e90659.
(16) O'Nuallain, B., Williams, A. D., Westermark, P., and Wetzel, R. (2004) Seeding specificity in amyloid growth induced by heterologous fibrils. *J. Biol. Chem. 279*, 17490−17499.
(17) Krebs, M. R., Morozova-Roche, L. A., Daniel, K., Robinson, C. V., and Dobson, C. M. (2004) Observation of sequence specificity in the seeding of protein amyloid fibrils. *Protein Sci. 13*, 1933−1938.
(18) Polymeropoulos, M. H., Lavedan, C., Leroy, E., Ide, S. E., Dehejia, A., Dutra, A., Pike, B., Root, H., Rubenstein, J., Boyer, R., Stenroos, E. S., Chandrasekharappa, S., Athanassiadou, A., Papapetropoulos, T., Johnson, W. G., Lazzarini, A. M., Duvoisin, R. C., Di Iorio, G., Golbe, L. I., and Nussbaum, R. L. (1997) Mutation in the alpha-synuclein gene identified in families with Parkinson's disease. *Science 276*, 2045−2047.
(19) Kruger, R., Kuhn, W., Muller, T., Woitalla, D., Graeber, M., Kosel, S., Przuntek, H., Epplen, J. T., Schols, L., and Riess, O. (1998) Ala30Pro mutation in the gene encoding alpha-synuclein in Parkinson's disease. *Nat. Genet. 18*, 106−108.
(20) Zarranz, J. J., Alegre, J., Gomez-Esteban, J. C., Lezcano, E., Ros, R., Ampuero, I., Vidal, L., Hoenicka, J., Rodriguez, O., Atares, B., Llorens, V., Tortosa, E. G., del Ser, T., Munoz, D. G., and de Yebenes, J. G. (2004) The new mutation, E46K, of alpha-synuclein causes Parkinson and Lewy body dementia. *Ann. Neurol. 55*, 164−173.
(21) Proukakis, C., Dudzik, C. G., Brier, T., MacKay, D. S., Cooper, J. M., Millhauser, G. L., Houlden, H., and Schapira, A. H. (2013) A novel alpha-synuclein missense mutation in Parkinson disease. *Neurology 80*, 1062−1064.
(22) Lesage, S., Anheim, M., Letournel, F., Bousset, L., Honore, A., Rozas, N., Pieri, L., Madiona, K., Durr, A., Melki, R., Verny, C., and Brice, A. (2013) G51D alpha-synuclein mutation causes a novel parkinsonian-pyramidal syndrome. *Ann. Neurol. 73*, 459−471.
(23) Pasanen, P., Myllykangas, L., Siitonen, M., Raunio, A., Kaakkola, S., Lyytinen, J., Tienari, P. J., Poyhonen, M., and Paetau, A. (2014) A novel alpha-synuclein mutation A53E associated with atypical multiple system atrophy and Parkinson's disease-type pathology. *Neurobiol. Aging 35*, 2180.e1−2180.e5.
(24) Yonetani, M., Nonaka, T., Masuda, M., Inukai, Y., Oikawa, T., Hisanaga, S., and Hasegawa, M. (2009) Conversion of wild-type alpha-synuclein into mutant-type fibrils and its propagation in the presence of A30P mutant. *J. Biol. Chem. 284*, 7940−7950.
(25) Giasson, B. I., Forman, M. S., Higuchi, M., Golbe, L. I., Graves, C. L., Kotzbauer, P. T., Trojanowski, J. Q., and Lee, V. M. (2003) Initiation and synergistic fibrillization of tau and alpha-synuclein. *Science 300*, 636−640.
(26) Kotzbauer, P. T., Giasson, B. I., Kravitz, A. V., Golbe, L. I., Mark, M. H., Trojanowski, J. Q., and Lee, V. M. (2004) Fibrillization of alpha-synuclein and tau in familial Parkinson's disease caused by the A53T alpha-synuclein mutation. *Exp. Neurol. 187*, 279−288.
(27) Guo, J. L., Covell, D. J., Daniels, J. P., Iba, M., Stieber, A., Zhang, B., Riddle, D. M., Kwong, L. K., Xu, Y., Trojanowski, J. Q., and Lee, V. M. (2013) Distinct alpha-synuclein strains differentially promote tau inclusions in neurons. *Cell 154*, 103−117.
(28) Paravastu, A. K., Leapman, R. D., Yau, W. M., and Tycko, R. (2008) Molecular structural basis for polymorphism in Alzheimer's beta-amyloid fibrils. *Proc. Natl. Acad. Sci. U. S. A. 105*, 18349−18354.
(29) Tycko, R. (2014) Physical and structural basis for polymorphism in amyloid fibrils. *Protein Sci. 23*, 1528−1539.
(30) Heise, H., Hoyer, W., Becker, S., Andronesi, O. C., Riedel, D., and Baldus, M. (2005) Molecular-level secondary structure, polymorphism, and dynamics of full-length alpha-synuclein fibrils studied by solid-state NMR. *Proc. Natl. Acad. Sci. U. S. A. 102*, 15871−15876.
(31) Sidhu, A., Segers-Nolten, I., and Subramaniam, V. (2014) Solution conditions define morphological homogeneity of alpha-synuclein fibrils. *Biochim. Biophys. Acta, Proteins Proteomics 1844*, 2127−2134.
(32) Bousset, L., Pieri, L., Ruiz-Arlandis, G., Gath, J., Jensen, P. H., Habenstein, B., Madiona, K., Olieric, V., Bockmann, A., Meier, B. H., and Melki, R. (2013) Structural and functional characterization of two alpha-synuclein strains. *Nat. Commun. 4*, 2575.
(33) Giehm, L., Lorenzen, N., and Otzen, D. E. (2011) Assays for alpha-synuclein aggregation. *Methods 53*, 295−305.
(34) Grimsley, G. R., and Pace, C. N. (2003) Spectrophotometric Determination of Protein Concentration. *Current Protocols in Protein Science*, 3.1.1−3.1.9.
(35) Pinotsi, D., Buell, A. K., Galvagnion, C., Dobson, C. M., Kaminski Schierle, G. S., and Kaminski, C. F. (2014) Direct observation of heterogeneous amyloid fibril growth kinetics via two-color super-resolution microscopy. *Nano Lett. 14*, 339−345.
(36) Heldt, C. L., Zhang, S., and Belfort, G. (2011) Asymmetric amyloid fibril elongation: a new perspective on a symmetric world. *Proteins: Struct., Funct., Genet. 79*, 92−98.
(37) Wise-Scira, O., Aloglu, A. K., Dunn, A., Sakallioglu, I. T., and Coskuner, O. (2013) Structures and free energy landscapes of the wild-type and A30P mutant-type alpha-synuclein proteins with dynamics. *ACS Chem. Neurosci. 4*, 486−497.
(38) Heise, H., Celej, M. S., Becker, S., Riedel, D., Pelah, A., Kumar, A., Jovin, T. M., and Baldus, M. (2008) Solid-state NMR reveals structural differences between fibrils of wild-type and disease-related A53T mutant alpha-synuclein. *J. Mol. Biol. 380*, 444−450.
(39) Esler, W. P., Stimson, E. R., Jennings, J. M., Vinters, H. V., Ghilardi, J. R., Lee, J. P., Mantyh, P. W., and Maggio, J. E. (2000) Alzheimer's disease amyloid propagation by a template-dependent dock-lock mechanism. *Biochemistry 39*, 6288−6295.
(40) Straub, J. E., and Thirumalai, D. (2011) Toward a molecular theory of early and late events in monomer to amyloid fibril formation. *Annu. Rev. Phys. Chem. 62*, 437−463.
(41) Qiang, W., Kelley, K., and Tycko, R. (2013) Polymorph-specific kinetics and thermodynamics of beta-amyloid fibril growth. *J. Am. Chem. Soc. 135*, 6860−6871.
(42) Hoyer, W., Cherny, D., Subramaniam, V., and Jovin, T. M. (2004) Rapid self-assembly of alpha-synuclein observed by in situ atomic force microscopy. *J. Mol. Biol. 340*, 127−139.
(43) Wordehoff, M. M., Bannach, O., Shaykhalishahi, H., Kulawik, A., Schiefer, S., Willbold, D., Hoyer, W., and Birkmann, E. (2015) Single fibril growth kinetics of alpha-synuclein. *J. Mol. Biol. 427*, 1428−1435.

DOI: 10.1021/acschemneuro.5b00322
ACS Chem. Neurosci. 2016, 7, 719−727

(44) Ban, T., Hoshino, M., Takahashi, S., Hamada, D., Hasegawa, K., Naiki, H., and Goto, Y. (2004) Direct observation of Abeta amyloid fibril growth and inhibition. *J. Mol. Biol. 344*, 757−767.
(45) Carulla, N., Caddy, G. L., Hall, D. R., Zurdo, J., Gairi, M., Feliz, M., Giralt, E., Robinson, C. V., and Dobson, C. M. (2005) Molecular recycling within amyloid fibrils. *Nature 436*, 554−558.
(46) Goldsbury, C., Kistler, J., Aebi, U., Arvinte, T., and Cooper, G. J. (1999) Watching amyloid fibrils grow by time-lapse atomic force microscopy. *J. Mol. Biol. 285*, 33−39.
(47) Scheibel, T., Kowal, A. S., Bloom, J. D., and Lindquist, S. L. (2001) Bidirectional amyloid fiber growth for a yeast prion determinant. *Curr. Biol. 11*, 366−369.
(48) Baiesi, M., Seno, F., and Trovato, A. (2011) Fibril elongation mechanisms of HET-s prion-forming domain: topological evidence for growth polarity. *Proteins: Struct., Funct., Genet. 79*, 3067−3081.
(49) DePace, A. H., and Weissman, J. S. (2002) Origins and kinetic consequences of diversity in Sup35 yeast prion fibers. *Nat. Struct. Biol. 9*, 389−396.
(50) Dedmon, M. M., Lindorff-Larsen, K., Christodoulou, J., Vendruscolo, M., and Dobson, C. M. (2005) Mapping long-range interactions in alpha-synuclein using spin-label NMR and ensemble molecular dynamics simulations. *J. Am. Chem. Soc. 127*, 476−477.
(51) Lee, J. C., Lai, B. T., Kozak, J. J., Gray, H. B., and Winkler, J. R. (2007) Alpha-synuclein tertiary contact dynamics. *J. Phys. Chem. B 111*, 2107−2112.
(52) Chiti, F., Stefani, M., Taddei, N., Ramponi, G., and Dobson, C. M. (2003) Rationalization of the effects of mutations on peptide and protein aggregation rates. *Nature 424*, 805−808.
(53) Krasnoslobodtsev, A. V., Peng, J., Asiago, J. M., Hindupur, J., Rochet, J. C., and Lyubchenko, Y. L. (2012) Effect of spermidine on misfolding and interactions of alpha-synuclein. *PLoS One 7*, e38099.
(54) Longair, M. H., Baker, D. A., and Armstrong, J. D. (2011) Simple Neurite Tracer: open source software for reconstruction, visualization and analysis of neuronal processes. *Bioinformatics 27*, 2453−2454.

DOI: 10.1021/acschemneuro.5b00322
ACS Chem. Neurosci. 2016, 7, 719−727